Navier-Stokes Simulation of Three-Dimensional Hypersonic Equilibrium Flows with Ablation

P. D. Thomas* and K. L. Neier†
Lockheed Missiles & Space Company, Inc.
Palo Alto, California 94304

The paper describes the theory underlying the Hypersonic Equilibrium Ablative Re-entry Three-dimensional Simulation (HEARTS) code, a numerical simulation of the re-entry heating environment. The unsteady, Navier-Stokes equations are applied to equilibrium mixtures of air and foreign gases produced by ablation. The bow shock wave is fitted as a sharp, free-boundary surface with shock-slip boundary conditions for high-altitude flow. Wall boundary conditions on segmented heatshields of different materials allow for mass injection and body spin with an adiabatic wall or a prescribed temperature distribution. A slip model is included for rarefied flow. The numerical method is patterned after the Beam-Warming alternating direction implicit (ADI) scheme with a finite-volume discretization, implicit boundary conditions, and a moving grid. The code has two unified modes of operation: a zonal mode for flows where upstream influence is significant and a time-iterative spatial marching mode for flows where it is not.

Introduction

HYPERSONIC flows with real-gas effects are important for design of vehicles that re-enter the atmosphere in a variety of missions, ranging from ballistic missiles and low-orbit spacecraft such as the Space Shuttle, to high-speed, orbital-transfer vehicles. Laboratory simulation of these hypersonic flows often is not possible or is incomplete, and flight tests are expensive and time consuming. Numerical simulations are assuming an important role as cost-effective complements to laboratory and flight tests.

This paper describes the Hypersonic Equilibrium Ablative Re-entry Three-dimensional Simulation (HEARTS) code, a computational tool aimed at numerical simulation of the hypersonic heating environment, including the effects of heat-shield ablation, encountered by re-entering vehicles within the flight regime where the flow remains near thermochemical equilibrium. The equations, boundary conditions, and numerical methods underlying the HEARTS code are presented. Numerical results are restricted to an illustrative case. Detailed numerical results for a variety of flows are given in a series of summary reports.[1] These include flows over multiconic bodies, bodies with indented nose tips, and bodies with surface gouges at the juncture between dissimilar heat-shield materials. A number of these cases contain comparisons with experimental data to support the validity of the numerical simulations.

Equations and Boundary Conditions

Equations

The numerical simulation technique is based on the complete, three-dimensional, Navier-Stokes equations applied to equilibrium mixtures of air and foreign gases produced by body-surface ablation. The classical compressible Navier-Stokes equation apply only to gases with a single component species. For a multispecies mixture, the global mass, momentum, and energy equations for the mixture are supplemented by a set of species mass conservation equations that include diffusion terms and chemical production rate source terms in addition to the convection terms that appear in the global mass conservation equation. The chemical production rate terms cannot be ignored, even though the mixture is considered to be in local thermochemical equilibrium at each point in the flow. Moreover, the global energy conservation equation for the mixture includes additional terms to account for the energy transported by mass diffusion of species.[2]

Great simplifications occur under the approximation that all species have a Lewis number *Le* of unity. The diffusive mass transport terms in the global-energy conservation equation may be combined with the thermal-conduction term in such a way that enthalpy rather than the temperature becomes the potential that drives thermal heat flux.[3] Further, the species conservation equations may be combined into a set of homogeneous (source-free) equations for the mass concentrations C of the individual chemical elements of which the species mixture is composed.[4] This work addresses gas mixtures evolved by ablation of segmented heat-shields consisting of at most a few materials, but each material may have a complex chemical composition. It is a further consequence of the unity Lewis number approximation that the solution to the element conservation equations may be constructed by solving a similar set of equations that govern diffusion of individual wall materials injected into the gas mixture. This approach reduces the total number of equations because the number of distinct materials is generally smaller than the number of chemical elements in the mixture of ablative and freestream gases. Because the element transport equations and their boundary conditions are linear in C, each element mass fraction $C_k(x,t)$ can be written as a linear combination of the mass fractions $C_n(x,t)$ of wall materials in the gas mixture and of the local mass fraction $C_f(x,t)$ of the freestream gas

$$C_k(x,t) = C_{\infty k} + \sum_{n=1}^{N} (C_{nsk} - C_{\infty k}) C_n(x,t) \tag{1a}$$

$$C_f = 1 - \sum_{n=1}^{N} C_n \tag{1b}$$

where $C_{\infty k}$ is the mass fraction of element k in the freestream gas, C_{nsk} is the mass fraction of element k in the nth solid-wall material, and N is the total number of distinct ablative wall materials comprising the body surface.

The equations to be solved thus consist of a small number of ablative material conservation equations with convective and diffusive transport terms and the Navier-Stokes equations for the global mixture of freestream and ablative gases. These are supplemented by the equilibrium equation of state for pressure p, temperature T, and enthalpy h as functions of the mixture thermodynamic state variables density ρ, specific in-

Presented as Paper 89-1650 at the AIAA 24th Thermophysics Conference, Buffalo, NY, June 12-14, 1989; received July 31, 1989; revision received Nov. 10, 1989.

*Senior Staff Scientist, Research & Development Division. Associate Fellow AIAA.

†Research Scientist, Research & Development Division.

ternal energy e, and local composition C.

$$p=(\gamma-1)\rho e, \qquad h=\gamma e \tag{2a}$$

$$\gamma=\gamma\ (\rho,e,C_k), \qquad T=T(\rho,e,C_k) \qquad k=1,2,\ldots \tag{2b}$$

Similar relations define the transport properties, viscosity $\bar{\mu}$, Prandtl number Pr, and Schmidt number Sc.

The governing equations are written first in a Cartesian coordinate system in which $\boldsymbol{x}$ is the radius vector and $\boldsymbol{u}$ is the corresponding velocity vector

$$\boldsymbol{x}=(x_1,x_2,x_3) \qquad \boldsymbol{u}=(u_1,u_2,u_3) \tag{3}$$

then are reformulated in strong conservation-law form in terms of a general curvilinear coordinate system (ξ_1, ξ_2, ξ_3) through a general time-dependent transformation of the independent variables (x_i,t)

$$\xi_i=\xi_i(\boldsymbol{x},t), \qquad \tau=t \tag{4}$$

but the original Cartesian momentum components ρu_i are retained as dependent variables.

The metric quantities of the transformation are

$$\nabla\xi_i=\frac{\partial\boldsymbol{x}}{\partial\xi_j}\times\frac{\partial\boldsymbol{x}}{\partial\xi_k} \tag{5a}$$

$$\frac{\partial\xi_i}{\partial t}=-\frac{\partial\boldsymbol{x}}{\partial\tau}\cdot\nabla\xi_i \tag{5b}$$

$$\frac{\partial\boldsymbol{x}}{\partial\tau}=-J^{-1}\frac{\partial\boldsymbol{x}}{\partial\xi_i}\frac{\partial\hat{\xi}_i}{\partial t} \tag{5c}$$

where ∇ denotes the classical Cartesian gradient vector operator, the caret denotes multiplication by J

$$\frac{\partial\hat{\xi}_i}{\partial t}=J\frac{\partial\xi_i}{\partial t}, \qquad \nabla\hat{\xi}_i=J\nabla\xi_i \tag{5d}$$

and J denotes the Jacobian determinant of the inverse transformation

$$J=\left|\frac{\partial x_i}{\partial\xi_j}\right|=\frac{\partial\boldsymbol{x}}{\partial\xi_i}\cdot\frac{\partial\boldsymbol{x}}{\partial\xi_j}\times\frac{\partial\boldsymbol{x}}{\partial\xi_k} \tag{5e}$$

where cyclic permutation of the subscripts i, j, k is implied.

The following identities are satisfied analytically by the metric quantities

$$\frac{\partial(\nabla\hat{\xi}_i)}{\partial\xi_i}=0 \tag{6a}$$

$$\frac{\partial J}{\partial\tau}+\frac{\partial}{\partial\xi_i}\left(\frac{\partial\hat{\xi}_i}{\partial t}\right)=0 \tag{6b}$$

Equation (6b) is a differential statement of the geometric conservation law (GLC),[5] which must be taken into account in solving the equations numerically on moving grids that accommodate the motion of free boundaries such as the outer bow shock wave.

In terms of the curvilinear coordinates, the governing equations have the following form:

Navier Stokes:

$$\frac{\partial(J\boldsymbol{q})}{\partial\tau}+\frac{\partial}{\partial\xi_i}\left(\boldsymbol{q}\frac{\partial\hat{\xi}_i}{\partial t}+\hat{\boldsymbol{f}}_i\right)=Re^{-1}\frac{\partial\hat{\boldsymbol{\omega}}_i}{\partial\xi_i} \tag{7}$$

Material Transport:

$$\frac{\partial(J\boldsymbol{d})}{\partial\tau}+\frac{\partial}{\partial\xi_i}\left[\left(\frac{\partial\hat{\xi}_i}{\partial t}+\hat{u}_i\right)\boldsymbol{d}\right]=Re^{-1}\frac{\partial\boldsymbol{\phi}_i}{\partial\xi_i} \tag{8}$$

where repeated indices imply summation; the inviscid flux vector $\hat{\boldsymbol{f}}_i$ and advection velocity $\hat{u}_i$ are

$$\hat{\boldsymbol{f}}_i=\rho\hat{u}_i(1,\boldsymbol{u},H)^T+p(0,\nabla\hat{\xi}_i,0)^T, \qquad \hat{u}_i=\boldsymbol{u}\cdot\nabla\hat{\xi}_i$$

$$H=E+p/\rho, \qquad E=e+\boldsymbol{u}^2/2, \qquad \boldsymbol{q}=\rho(1,\boldsymbol{u},E)^T \tag{9a}$$

and where the following is a vector of ablative material densities.

$$\boldsymbol{d}=\rho C=(\rho_1,\rho_2,\ldots\rho_n,\ldots)^T$$

The equations are given in dimensionless form with densities, temperature, velocity, and viscosity normalized by their freestream values; pressure is normalized by the freestream momentum flux $\rho_\infty u_\infty^2$; specific energy and enthalpy are normalized by u_∞^2; dimensions are normalized by a characteristic body length L; time is normalized by L/u_∞. It follows that the Reynolds number Re is defined in terms of freestream conditions and the characteristic length L.

The viscous flux vector $\hat{\omega}$ separates naturally into three parts, one of which involves only spatial unidirectional derivatives with respect to ξ_i. The other two parts involve only cross derivatives with respect to the transverse directions ξ_j and ξ_k.

$$\hat{\boldsymbol{\omega}}_i=\hat{\boldsymbol{\omega}}_i^i+\hat{\boldsymbol{\omega}}_i^j+\hat{\boldsymbol{\omega}}_i^k \tag{9b}$$

$$\hat{\boldsymbol{\omega}}_i^i=\bar{\mu}J^{-1}\left[0,\hat{\boldsymbol{\sigma}}_i^i,|\nabla\hat{\xi}_i|^2Pr^{-1}\frac{\partial h}{\partial\xi_i}+\boldsymbol{u}\cdot\hat{\boldsymbol{\sigma}}_i^i\right]^T \tag{9c}$$

$$\hat{\boldsymbol{\omega}}_i^j=\bar{\mu}J^{-1}\left[0,\hat{\boldsymbol{\sigma}}^j,(\nabla\hat{\xi}_i\cdot\nabla\hat{\xi}_j)Pr^{-1}\frac{\partial h}{\partial\xi_j}+\boldsymbol{u}\cdot\hat{\boldsymbol{\sigma}}_i^j\right]^T \tag{9d}$$

$$\hat{\boldsymbol{\sigma}}_i^i=|\nabla\hat{\xi}_i|^2\frac{\partial\boldsymbol{u}}{\partial\xi_i}+\frac{1}{3}\left(\nabla\hat{\xi}_i\cdot\frac{\partial\boldsymbol{u}}{\partial\xi_i}\right)\nabla\hat{\xi}_i \tag{9e}$$

$$\hat{\boldsymbol{\sigma}}_i^j=(\nabla\hat{\xi}_i\cdot\nabla\hat{\xi}_j)\frac{\partial\boldsymbol{u}}{\partial\xi_j}+\left(\nabla\hat{\xi}_i\cdot\frac{\partial\boldsymbol{u}}{\partial\xi_j}\right)\nabla\hat{\xi}_j-\frac{2}{3}\left(\nabla\hat{\xi}_j\cdot\frac{\partial\boldsymbol{u}}{\partial\xi_j}\right)\nabla\hat{\xi}_i \tag{9f}$$

Similarly, the diffusion flux vector $\boldsymbol{\phi}_i$ may be separated into unidirectional-derivative and cross-derivative parts

$$\boldsymbol{\phi}_i=\boldsymbol{\phi}_i^i+\boldsymbol{\phi}_i^j+\boldsymbol{\phi}_i^k \tag{10a}$$

$$\boldsymbol{\phi}_i^i=\bar{\mu}\ (ScJ)^{-1}|\nabla\hat{\xi}_i|^2\frac{\partial(\boldsymbol{d}/\rho)}{\partial\xi_i} \tag{10b}$$

$$\boldsymbol{\phi}_i^j=\bar{\mu}\ (ScJ)^{-1}(\nabla\hat{\xi}_i\cdot\nabla\hat{\xi}_j)\frac{\partial(\boldsymbol{d}/\rho)}{\partial\xi_j} \tag{10c}$$

In Eqs. (9) and (10), there is no summation on repeated indices, and cyclic permutation of indices i, j, k is implied. Expressions for the other cross-derivative terms, $\hat{\boldsymbol{\omega}}_i^k$, $\hat{\boldsymbol{\sigma}}_i^k$, $\hat{\boldsymbol{\phi}}_i^k$, may be obtained from Eqs. (9d), (9f), and (10c) by the substitution $j\rightarrow k$.

Boundary Conditions

The foregoing equations are applied in the shock-layer region lying between the body surface and the outer-bow shock wave. We take (ξ_1, ξ_2, ξ_3) to be boundary-conforming curvilinear coordinates such that the body and bow shock are surfaces $\xi_3=$const, ξ_1 is the general streamwise coordinate, and $\xi_2=\xi_2(\phi)$ is the circumferential coordinate. The body, shock, and symmetry planes are natural boundaries, but it is necessary to introduce artificial boundaries as well. The flow over the forward part of a blunt body, excluding the wake, may be computed by introducing an artificial outflow boundary that limits the numerical solution to a finite-spatial region. A similar artificial inflow boundary may be used ahead of the outflow boundary to confine the flow calculation to a streamwise

zone in cases where upstream influence is weak near the inflow boundary.

Body Surface

The boundary condition at the body surface $\xi_3 = \text{const}$ allows for body spin about the Cartesian x_1-axis and surface-normal mass injection to simulate surface ablation. The no-slip, surface-velocity boundary condition then is

$$\boldsymbol{u} = (\dot{m}/\rho)\nabla\xi_3/|\nabla\xi_3| + 2\pi\dot{w}\boldsymbol{R}\times\boldsymbol{e}_1 \tag{11}$$

where $\dot{m}$ is the dimensionless mass injection rate, and $\dot{w}$ is the dimensionless spin rate in rad/s referred to the ratio u_∞/L, $\boldsymbol{R} = (0, x_2, x_3)$, and $\boldsymbol{e}_1 = (1, 0, 0)$. The thermal-boundary condition allows for either a prescribed wall temperature distribution $T = T_w(\xi_1, \xi_2)$ or an adiabatic wall in which the convective energy transport of the injected gas balances the thermal heat flux to the wall

$$\dot{m}H - \bar{\mu}(RePrJ|\nabla\hat{\xi}_3|)^{-1}\nabla\hat{\xi}_3\cdot(\nabla\hat{\xi}_i\partial h/\partial\xi_i) = 0, \qquad H \approx h \tag{12}$$

A similar balance between convection and diffusion forms the surface-boundary conditions for the ablative material mass conservation [Eq. (8)].

$$\dot{m}C_n - \bar{\mu}\,(ReScJ|\nabla\hat{\xi}_3|)^{-1}\nabla\hat{\xi}_3\cdot(\nabla\hat{\xi}_i\partial C_n/\partial\xi_i) = \dot{m}C_{ns} \tag{13}$$

where $C_{ns}(\xi_1, \xi_2)$ denotes the normalized mass concentration of material n at the wall. It is defined to be unity at points (ξ_1, ξ_2) where the wall is composed of material n and to be zero elsewhere.

The HEARTS code also contains velocity-slip and temperature-slip boundary conditions for rarefied flow over nonablating surfaces.[6]

Bow Shock

The bow shock wave is fitted as a sharp, free boundary surface $\xi_3 = \text{const}$ across which the flow variables are discontinuous. The shock-jump relations are applied as boundary conditions at this surface. These relations may be obtained by integrating the governing Eqs. (7) and (8) across a small interval $\nabla\xi_3$ that encloses the shock surface.

$$\boldsymbol{q}\dot{\xi}_i + \hat{\boldsymbol{f}}_i - Re^{-1}\hat{\boldsymbol{\omega}}_i^j = \boldsymbol{q}_\infty\dot{\xi}_i + \hat{\boldsymbol{f}}_{i\infty} - Re^{-1}\boldsymbol{\omega}_{i\infty}^j, \qquad i = 3 \tag{14}$$

$$(\dot{\xi}_i + \hat{u}_i)\boldsymbol{d} - Re^{-1}\boldsymbol{\phi}_i^j = (\dot{\xi}_i + \hat{u}_{i\infty})\boldsymbol{d}_\infty - Re^{-1}\boldsymbol{\phi}_{i\infty}^j, \qquad i = 3 \tag{15}$$

where $\dot{\xi} = \partial\hat{\xi}_i/\partial t$. The freestream is assumed to be spatially uniform so that the viscous stress vector and diffusion flux vector vanish

$$\boldsymbol{\omega}_{i\infty}^j = \boldsymbol{\phi}_{i\infty}^j = 0 \tag{16}$$

The metric quantity $\dot{\xi} = \partial\hat{\xi}_3/\partial t$ in Eqs. (14) and (15) represents a shock-speed parameter that determines the physical shock velocity $\partial x/\partial\tau$ from Eq. (6b). The shock is the only moving boundary, in which case

$$\frac{\partial\hat{\xi}_1}{\partial t} = \frac{\partial\hat{\xi}_2}{\partial t} = 0, \qquad \dot{\xi} = \frac{\partial\hat{\xi}_3}{\partial t} \neq 0 \tag{17}$$

At sufficiently high Reynolds numbers and moderate mass injection rates, the injected gases remain confined to a thin wall layer well inside the shock, and the jump equation [Eq. (15)] may be approximated by the simpler boundary condition $C_n \simeq C_{n\infty}$.

The shock jump relations of Eq. (14) embody viscous terms, often referred to loosely as shock-slip terms that afford an improved approximation for rarefied flow effects encountered at high altitudes. The classical inviscid jump relations are recovered from Eq. (14) in the limit $Re \to \infty$.

Inflow Boundary

When the inflow is predominantly supersonic, except in a thin viscous wall boundary layer, all inflow variables are prescribed, and the streamwise stress and fluxes are assumed to vanish

$$\frac{\partial\hat{\boldsymbol{\omega}}_i^j}{\partial\xi_i} = \frac{\partial\boldsymbol{\phi}_i^j}{\partial\xi_i} = 0 \qquad \text{for } i = 1 \tag{18}$$

This is equivalent to a continuative boundary condition where the streamwise viscous stress, heat flux, and diffusion flux tend toward constant levels as one approaches the inflow boundary.

Outflow Boundary

The outflow is presumed to be supersonic except in a thin wall boundary layer, and no boundary conditions are imposed on the flow variables. The continuative boundary conditions [Eq. (18)] are imposed on the streamwise stress, heat flux, and diffusion flux.

Turbulence

Flow turbulence effects are accounted for through an eddy viscosity $\bar{\mu}_t$ that is added to the molecular viscosity $\bar{\mu}_m$ and through a turbulent Prandtl number Pr_t that is used to form the total thermal energy transport coefficient. The quantities $\bar{\mu}_t$, Pr_t are obtained from an algebraic turbulence model that is basically the one developed by Baldwin and Lomax[7] with several modifications to adapt it to hypersonic flows with surface mass injection.[8]

Numerical Method

The numerical method is patterned after the Beam-Warming/Briley-MacDonald alternating direction implicit (ADI) scheme[9,10] with modifications to employ a spatially second-order accurate finite-volume discretization of the equations, fully implicit boundary conditions, and a moving grid linked to motion of the bow shock wave.[5] Finite-volume analogs of the equations and boundary conditions are solved on a grid that is uniform in each of the three directions

$$\xi_i = (j_i - 1)\Delta\xi_i, \qquad 1 \le j_i \le J_i \tag{19a}$$

$$\Delta\xi_i = 1 \tag{19b}$$

Zonal Solutions for General Regions

First, we present the difference equations that would apply if the shock and grid were stationary, and then we outline the modifications required to account for shock and grid motion. We deal separately with the equations for interior and boundary grid points.

Stationary Shock and Grid: Interior Points

For interior grid points, we employ the Beam-Warming/Briley-MacDonald algorithm,[9,10] in which the spatial derivative terms in Eqs. (7) and (8) are represented by second-order accurate centered differences, and the time differencing is performed implicitly. Thomas and Lombard[5] have shown that the resulting difference equations are identical to those obtained by applying the finite-volume method in the computational space, that is, by applying the integral form of the flow conservation equations to a cubical cell of volume $\Delta V = \Delta\xi_1\,\Delta\xi_2\,\Delta\xi_3$ that encloses each interior grid point of the computational space. We employ the finite-volume method because it facilitates the development of implicit or explicit boundary-

point difference equations that are compatible with the interior-point equations.

The equations can be represented conveniently in terms of classical central difference operators. Let E denote the classical shift operator, which acts to shift the index j of a general mesh function f_j

$$Ef_j = f_{j+1}, \qquad E^{-1}f_j = f_{j-1}, \qquad E^{\pm 1/2}f_j = f_{j\pm 1/2} \tag{20}$$

Then, the central operators δ, μ are defined as

$$\delta = E^{1/2} - E^{-1/2} \tag{21a}$$

$$\mu = (E^{1/2} + E^{-1/2})/2 \tag{21b}$$

$$\mu\delta = (E - E^{-1})/2 \tag{21c}$$

These difference operators allow the discretized form of Eq. (7) to be written in the form

$$J\frac{\partial \boldsymbol{q}}{\partial \tau} + \mu\delta\left[\hat{\boldsymbol{f}}_i - Re^{-1}(\hat{\omega}_i^j + \hat{\omega}_i^k)\right] - Re^{-1}\delta\hat{\omega}_i^j = 0 \tag{22}$$

where the mesh increments $\Delta\xi_j$ do not appear explicitly because of Eq. (19b) and where the indices i, j, k are understood to be permuted cyclically. In the viscous terms of Eq. (22), the operator δ is used to represent the spatial derivatives $\partial/\partial\xi_i$ that appear in the last term, whereas the operator $\mu\delta$ is used to represent $\partial/\partial\xi_j$, $\partial/\partial\xi_k$ in the remaining terms ω_i^j, ω_i^k, respectively. The central difference operator $\mu\delta$ also is used to represent the spatial derivatives that appear in Eqs. (5) and (6) for the metric quantities. The resulting difference equations violate the metric identity [Eq. (6a)], but this defect can be overcome by first recasting Eq. (5a) in the following conservative form[5]

$$\nabla\hat{\xi}_i = \frac{1}{2}\left[\frac{\partial}{\partial\xi_j}\left(\boldsymbol{x}\times\frac{\partial \boldsymbol{x}}{\partial\xi_k}\right) + \frac{\partial}{\partial\xi_k}\left(\frac{\partial \boldsymbol{x}}{\partial\xi_j}\times\boldsymbol{x}\right)\right] \tag{23}$$

before applying the spatial difference operator $\mu\delta$ to represent each spatial derivative.

The ablative material transport equation [Eq. (8)] is discretized in similar fashion, except that an upwind formula is used to evaluate the advective flux $(\hat{u}_j\, \boldsymbol{d})$ at the finite-volume cell faces $j \pm 1/2$. The resulting difference equation can be written as

$$J\frac{\partial \boldsymbol{d}}{\partial \tau} + \delta[(\mu\hat{u}_i)\boldsymbol{d}^{\pm} - Re^{-1}\boldsymbol{\phi}_i^j] - Re^{-1}\mu\delta(\boldsymbol{\phi}_i^j + \boldsymbol{\phi}_i^k) = 0 \tag{24a}$$

where the upwind-weighted material density is

$$\boldsymbol{d}_{j+1/2}^{\pm} = E^{1/2}[\mu - \beta\delta/2]\boldsymbol{d}, \qquad \beta = \mathrm{sgn}(u_i) \tag{24b}$$

and sgn is the algebraic sign function

$$\mathrm{sgn}(x) = x/|x| \tag{24c}$$

The spatial difference operators that enter into the three parts of the diffusion flux vector $\boldsymbol{\phi}$ in Eq. (10a) are the same as those in the corresponding parts of the viscous flux vector $\hat{\boldsymbol{\omega}}$ in Eq. (9). We are interested primarily in computing the steady-state flow as the time-asymptotic limit of an unsteady flow. Temporal accuracy is relatively unimportant, and we employ the simple, first-order, implicit-Euler time-differencing scheme for Eqs. (22) and (24) to obtain

$$J\frac{\Delta \boldsymbol{q}}{\Delta\tau} + \mu\delta\hat{\boldsymbol{f}}_i^{n+1} - Re^{-1}\delta(\hat{\omega}_i^j)^{n+1} - Re^{-1}\mu\delta(\hat{\omega}_i^j + \hat{\omega}_i^k)^n = 0 \tag{25}$$

$$J\frac{\Delta \boldsymbol{d}}{\Delta\tau} + \delta[(\mu\hat{u}_i)\boldsymbol{d}^{\pm} - Re^{-1}\boldsymbol{\phi}_i^j]^{n+1} - Re^{-1}\mu\delta(\boldsymbol{\phi}_i^j + \boldsymbol{\phi}_i^k)^n = 0 \tag{26}$$

where the superscript n denotes the time level, and Δ is the classical forward time-difference operator

$$\Delta\boldsymbol{q} = \boldsymbol{q}^{n+1} - \boldsymbol{q}^n, \qquad \Delta\tau = \tau^{n+1} - \tau^n$$

As in Ref. 9, the viscous and diffusive cross-derivative terms in Eqs. (25) and (26) are evaluated explicitly at time τ^n, whereas all other terms are evaluated implicitly at the advanced time τ^{n+1}. The latter advanced terms are linearized in time by using local Taylor series expansions.[11,12] The viscous terms $\hat{\omega}_i^j$ in Eq. (25) depend explicitly on spatial derivatives (differences) of $\boldsymbol{q}$. They also depend implicitly on both $\boldsymbol{q}$ and $\boldsymbol{d}$ through the state dependence of the transport properties $\tilde{\mu}$, Pr. These transport properties usually are approximated as locally constant in performing the linearization[9,11] without adverse effects on either accuracy or numerical stability. Under this approximation, the Navier-Stokes equation [Eq. (25)] is coupled to the material transport [Eq. (26)] only through the inviscid flux vector $\hat{\boldsymbol{f}}_i$. Under most conditions of present interest, we anticipate a weak dependence of the inviscid flux vector $\hat{\boldsymbol{f}}_i$ on the ablative material densities $\boldsymbol{d}$. We neglect this weak coupling, which permits Eqs. (25) and (26) to be solved in tandem rather than simultaneously. The linearized version of Eq. (25) then is

$$\left[\frac{J}{\Delta\tau}I + (\mu\delta F_i - Re^{-1}\delta W_i)^n\right]\Delta\boldsymbol{q} = \boldsymbol{r}^n \tag{27a}$$

where I denotes the identity matrix, F_i, W_i the inviscid and viscous flux Jacobian matrices, and r the residual

$$\boldsymbol{r}^n = -\left\{\mu\delta\hat{\boldsymbol{f}}_i - Re^{-1}[\delta\hat{\omega}_i^j + \mu\delta(\hat{\omega}_i^j + \hat{\omega}_i^k)]\right\}^n \tag{27b}$$

The described approach involves a two-stage solution procedure to advance the entire solution from τ^n to τ^{n+1}. The first is a frozen-flow stage in which we solve the linearized form [Eq. (27)] of the global mixture [Eq. (25)] as if the composition $\boldsymbol{d}$ were frozen (unchanging) over the time step. The second is a material-transport stage in which we solve Eq. (26) for $\boldsymbol{d}^{n+1}$ by using the updated flow variables $\boldsymbol{q}^{n+1}$ and the corresponding transport properties.

The solution is obtained by the ADI scheme.[9,10] For the global mixture equations [Eqs. (27)], this requires the solution of a 5×5 block-tridiagonal linear system in each direction. Solution of the ablative material transport equations requires much less computational work because the material densities $\boldsymbol{d}$ are mutually uncoupled. Only N scalar tridiagonal linear systems need be solved for the N material densities, and all of these tridiagonal systems have the same coefficients.

Artificial Numerical Dissipation

Artificial numerical dissipation terms are introduced in the Navier-Stokes equation to prevent nonlinear instabilities and to provide a dissipative mechanism for computing embedded shock waves.[9] We employ either one of two explicit artificial dissipation schemes: a conservative fourth-order scheme[12] or a dual second-order/fourth-order scheme.[13] No artificial dissipation is needed in the ablative material transport equations, because the upwind differencing scheme used for the advection term inherently has strong stability properties.

Boundary Conditions: Wall Boundary

The gasdynamic state variables at wall boundary points are determined from differenced forms of the wall-boundary conditions [Eqs. (11–13)]. Spatial derivatives in direction ξ_3, outward from the wall, are approximated by the spatial-forward

difference operator Δ

$$\partial/\partial\xi_3 \rightarrow \Delta_j = E - 1 \tag{28}$$

whereas transverse derivatives $\partial/\partial\xi_1$, $\partial/\partial\xi_2$ are approximated by the central-difference operator $\mu\delta$. It is assumed that the coordinate ξ_3 is nearly orthogonal to the wall in which case the transverse derivatives usually can be neglected, as can the normal pressure gradient $\partial p/\partial\xi_3 = 0$. The pressures then are equal at the wall point $j_3 = 1$ and the adjacent interior point

$$p_j^{n+1} = p_{j+1}^{n+1} \qquad \text{for} \qquad j = 1 \tag{29}$$

An implicit solution procedure is used in which the differenced forms of Eq. (29) and the wall-boundary conditions [Eq. (11) and (12)] are locally linearized in time. They are solved simultaneously with the interior-point equations in the body-normal ξ_3 sweep of the ADI sweep sequence during the initial frozen-composition stage of the computation, where the global mixture equations are solved. When the second material transport stage of the procedure is performed, the spatially differenced and linearized form of the boundary condition of Eq. (13) is solved simultaneously with the interior-point of Eqs. (26) during the ξ_3 sweep of the ADI sequence.

Outflow Boundary

Conditions at downstream outflow boundary points $j_1 = J_1$ are computed implicitly from difference equations obtained by applying the finite-volume technique to a boundary half-cell.[14] The resulting difference equations differ from the interior-point equations only in the terms for the streamwise direction $i = 1$. There, the operator $\mu\delta$ is replaced by $2\nabla_j$, where ∇_j is the backward difference operator defined by

$$\nabla_j = 1 - E^{-1}$$

The same operator ∇_j is used for derivatives $\partial/\partial\xi_1$ in Eqs. (6) for the metric quantities, and the viscous terms containing this type of derivative disappear from the outflow boundary point equations because of the continuative boundary condition [Eq. (18)].

Moving Shock and Grid

As stated earlier, the shock is a free boundary that moves in time as the flow solution evolves. Each ξ_3- directed coordinate line is presumed to remain stationary, and grid points move along the line as a function of time. The quantity $\partial \boldsymbol{x}/\partial\tau$ is the physical grid velocity, and $\partial s/\partial\tau = |\partial \boldsymbol{x}/\partial\tau|$ is the speed at which individual grid points move along the line. It is related to the grid-speed parameter through the equation

$$\dot{\xi} \triangleq \frac{\Delta}{\partial t}\frac{\partial \hat{\xi}_3}{} = -\frac{J}{|\partial \boldsymbol{x}/\partial\xi_3|}\frac{\mathrm{d}s}{\mathrm{d}\tau} \tag{30}$$

The grid speed parameter $\dot{\xi}$ at any interior point along the grid line is related to the corresponding value $\dot{\xi}_s$ at the shock through a preset stretching function S

$$J^{-1}\left|\frac{\partial \boldsymbol{x}}{\partial\xi_3}\right|\dot{\xi} = \left(J^{-1}\left|\frac{\partial \boldsymbol{x}}{\partial\xi_3}\right|\dot{\xi}\right)_s \cdot S(\xi_3) \tag{31}$$

An equation relating the grid speed parameter at the shock point $\dot{\xi}_s$ to the shock pressure can be obtained from the shock jump [Eq. (14)]. This equation accounts for shock-slip effects and can be written in the following form:

$$\dot{\xi} = b - [\boldsymbol{u}_\infty \cdot \nabla\hat{\xi}_3 + (b^2 + c + c' + c'')^{1/2}] \tag{32a}$$

$$b = (\gamma - 1)(Re\ Pr\ J)^{-1}|\nabla\hat{\xi}_3|^2\bar{\mu}\frac{\partial h}{\partial\xi_3}/p_\infty a \tag{32b}$$

$$c = \rho_\infty|\nabla\hat{\xi}_3|^2[(\gamma+1)P + (\gamma-1)](P-1)/2\rho_\infty a \tag{32c}$$

$$c' = -\gamma P(Re\ J)^{-1}(\boldsymbol{\sigma}\cdot\nabla\hat{\xi}_3)/\rho_\infty a \tag{32d}$$

$$c'' = (\gamma-1)(Re\ J)^{-2}(\boldsymbol{\sigma}\cdot\boldsymbol{\sigma})/2\rho_\infty p_\infty a \tag{32e}$$

$$a = P - \frac{\gamma - 1}{\gamma_\infty - 1}, \qquad P = p/p_\infty \tag{32f}$$

where $\boldsymbol{\sigma}$ denotes the viscous stress vector $\hat{\boldsymbol{\sigma}}_i^j$ as defined in Eq. (9e) with $i = 3$.

The grid motion enters into the flow equations through the first term in parentheses on the left-hand side of Eqs. (7) and (8). We employ a quasiconservative formulation in which all terms are retained in their strong-conservation form except for the time-derivative term and the term involving the grid speed $\dot{\xi}$. The quasiconservative form can be obtained from Eq. (7) by first expanding the derivatives of the first two terms using the rule for differentiating a product and then invoking the GCL [Eq. (6b)] to simplify the results. This yields

$$J\frac{\partial \boldsymbol{q}}{\partial\tau} + \dot{\xi}_i\frac{\partial \boldsymbol{q}}{\partial\xi_i} + \frac{\partial \hat{\boldsymbol{f}}_i}{\partial\xi_i} = Re^{-1}\frac{\partial\hat{\omega}_i}{\partial\xi_i} \tag{33}$$

The material transport [Eq. (8)] is reduced to quasiconservative form in similar fashion.

We then investigated two methods for solving Eqs. (30–33) simultaneously to obtain the shock conditions and grid speeds $\dot{\xi}$. In the first method, the grid speeds are lagged by one time step and are updated explicitly at the end of the time step. In the second method, which has much greater numerical stability, the grid speeds are computed implicitly. The implicit-difference equations for the shock-boundary points $j_3 = J_3 - 1$ incorporate the shock-boundary conditions [Eq. (14)] into the finite-volume equation for half-cells at the shock boundary and are then locally linearized.[8] The interior-point and shock-point equations are linearized with respect to the augmented vector of unknowns

$$\boldsymbol{Q} = (\boldsymbol{q}, \dot{\xi})^T \tag{34}$$

This gives a block-tridiagonal system of five equations in the six unknowns comprising the vector $\boldsymbol{Q}$. The sixth independent tridiagonal equation to close the system is obtained from Eq. (31) and the linearized form of Eq. (32).

The transverse ADI sweeps remain the same as for a stationary shock and grid, but the sweep over the ξ_3-direction requires the inversion of a 6×6 block-tridiagonal system for $\Delta\boldsymbol{Q}$. After the sweep is completed, the shock-speed parameter is updated along with the flow variables and one proceeds with the tandem solution to the ablative material conservation equations, taking into account the grid motion terms $(\dot{\xi}\partial\boldsymbol{d}/\partial\xi_3)^{n+1}$.

Convergence Acceleration

We have employed either one of two acceleration techniques: a progressive time step that is increased systematically during the iteration or a local time step that varies with position in the flowfield. The local time step is evaluated in terms of directionally averaged eigenvalues, where each eigenvalue is split into a convective part and a sound-speed part.[8]

Time-Iterative Marching Solutions

The preceding discussion has dealt with the algorithm used to perform zonal flow computations in which a time-dependent solution is carried out simultaneously at all grid points within a computational region, or zone. The complete zonal approach is necessary for mixed subsonic, transonic, and supersonic flow regions, such as the nose region of a blunt body or regions of massively separated flow caused by indentations,

ablation-induced surface gouges, or massive injection of ablation products. A more efficient time-iterative marching (TIM) algorithm has been devised for regions of predominantly supersonic flow where upstream influence is localized within a thin subsonic sublayer of the body surface boundary layer. The TIM algorithm uses the full machinery of the time-dependent zonal computation but applies it to a zone, whose width is a single mesh interval in the streamwise marching direction ξ_1 using an optional first-order or second-order spatial discretization of the equations in the marching direction.

The TIM difference equations differ from the zonal equations (25-27) as follows. All viscous terms that involve derivatives in the marching direction ξ_1 are omitted. For the inviscid terms with spatial derivatives in the marching direction ξ_1, we replace the central difference operator $\mu\delta$ by a two-parameter backward difference operator

$$\frac{\partial \hat{f}_1}{\partial \xi_1} \approx \tilde{\nabla} \hat{f}_1 = \theta'(\hat{f}_j^{n+1} - \hat{f}_{j-1}^{n}) - \theta''(\hat{f}_{j-1}^{n} - \hat{f}_{j-2}^{n}) \tag{35}$$

in which the constants $\theta' = 1$, $\theta'' = 0$ yield first-order accuracy and $\theta' = {}^3/_2$, $\theta'' = \frac{1}{2}$ yield second-order accuracy. Note that the only term that is evaluated implicitly at the advanced time is the one centered on the current marching station j, namely f_j^{n+1}. Upon linearization and approximate factorization of the implicit left-hand side operator, one obtains the following ADI sequence

$$\left(\frac{J}{\Delta\tau} I + \theta' F_1 + \mu\delta F_2 - Re^{-1}\delta W_2\right)^n \Delta\tilde{q}^{\,*} = \tilde{r}^n \tag{36a}$$

$$\left(\frac{J}{\Delta\tau} I + \theta' F_1 + \mu\delta F_3 - Re^{-1}\delta W_3\right)^n \Delta\tilde{q} = \left(\frac{J}{\Delta\tau} I + \theta' F_1\right)\Delta\tilde{q}^{\,*} \tag{36b}$$

$$q^{n+1} = q^n + \Delta\tilde{q} \tag{36c}$$

where $\tilde{r}^n$ differs from r^n in Eq. (27) only in that the centrally differenced inviscid term for the $i = 1$ direction is replaced by the backward difference in Eq. (35), and all viscous terms that involve spatial differences in the $i = 1$ direction are omitted.

The TIM equation (36) is applied iteratively in time n only at a single marching station j in the streamwise direction. The technique is comparable in computational eficiency to the parabolized Navier-Stokes (PNS) spatial marching technique,[16] but it avoids the accumulation of spatial marching errors by performing a few time iterations at each successive marching station, and no additional approximations are introduced to treat the pressure in the subsonic sublayer of the wall boundary layer.

Heat Transfer and Skin Friction

The skin friction and heat transfer at the wall are given by

$$s_w = -Re^{-1}\hat{\omega}_3 = -Re^{-1}(\hat{\omega}_3^1 + \hat{\omega}_3^2 + \hat{\omega}_3^3) \tag{37}$$

The first two terms in parentheses are transverse derivative terms that constitute a grid skewness correction to the skin friction and heat flux, and are computed to second-order accuracy by using the difference operator $\mu\delta$ to represent the transverse spatial derivatives. The third term in parentheses is the dominant term and must be computed with care. If this term were evaluated by using either first- or second-order one-sided difference formulas for the wall-normal derivative $\partial/\partial\xi_3$, the result would be inconsistent with the central-difference operators used for this term in obtaining the flowfield solution, and one could expect skin friction and heat transfer errors to arise from the inconsistency. To be consistent with the difference equations, we compute S_w by second-order-accurate extrapolation of $\ddot{\omega}_3^3$ from the nearest interior cell faces

$$[\hat{\omega}_3^3]_{j=1} = ({}^3/_2)[\hat{\omega}_3^3]_{j+\frac{1}{2}} - (\frac{1}{2})[\hat{\omega}_3^3]_{j+(3/2)} \tag{38}$$

Thermodynamic State and Transport Properties

We have used two methods to determine the equilibrium mixture equation of state and transport properties in Eqs. (2). For pure airflow or for a simple mixture of air and one ablative wall material of uniform elemental composition, the properties are obtained by an efficient table interpolation. For complex gas mixtures involving multiple heat shield materials, a full equilibrium computation is performed using a streamlined, vectorized version of the NASA Lewis CEC code.[15]

Numerical Simulation Results

The HEARTS code has been exercised extensively to predict the flowfield and surface heat transfer for both ablating and

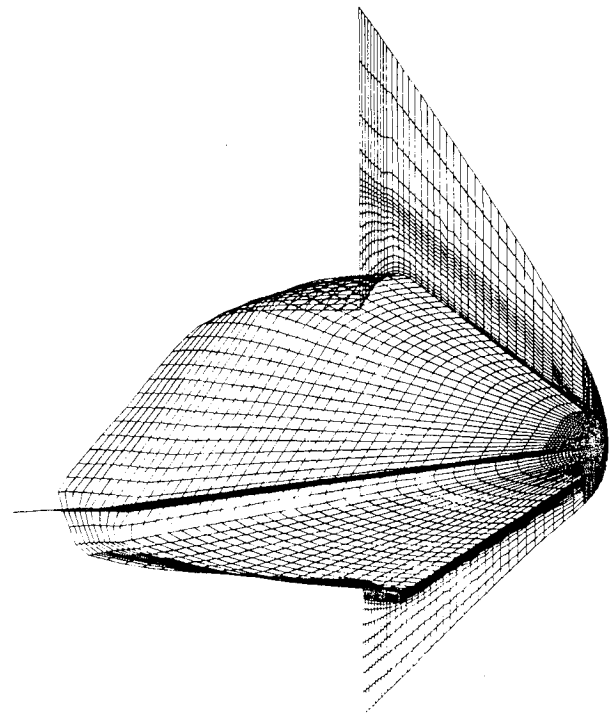

Fig. 1 Body surface and shock shape in windward, leeward, and midplanes of FDL-5A lifting body at 5-deg angle of attack.

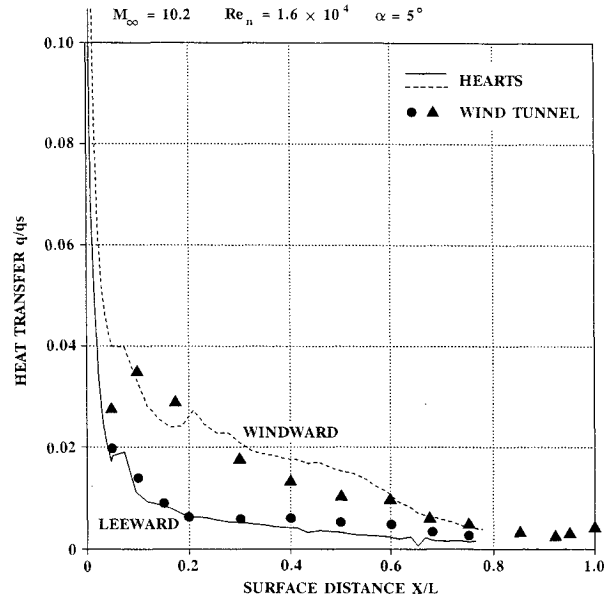

Fig. 2 FDL-5A body windward and leeward centerline heat transfer.

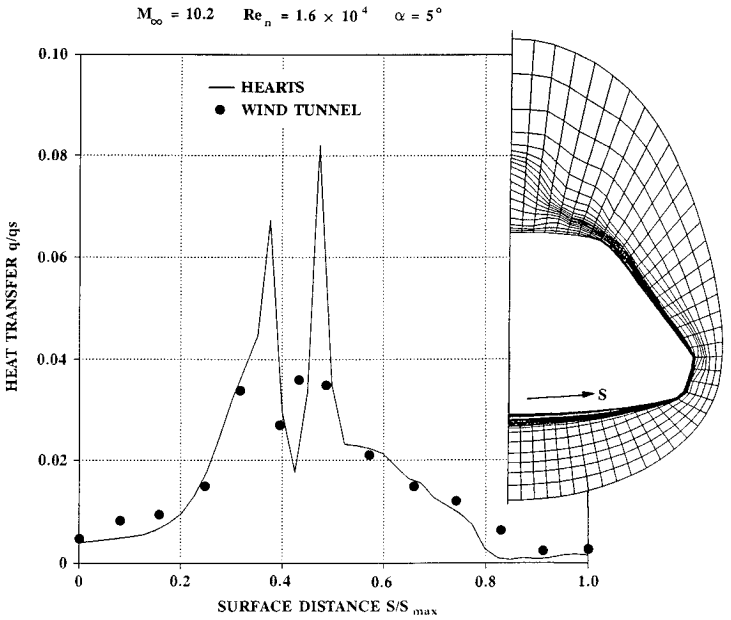

Fig. 3 FDL-5A body surface heat transfer at $X/L = 0.75$.

nonablating bodies having typical re-entry vehicle geometric configurations.[1] This includes axisymmetric configurations such as blunt multiconic bodies, indented nose-tip shapes, and bodies with local surface gouges at the juncture of dissimilar materials. We recently have extended the original code to have a unidirectional solution-adaptive grid[17] and an interface to the Air Force EAGLE grid-generator code.[18] We also have applied the extended code to three-dimensional flow about lifting bodies. Since numerical results for flow about ablating bodies have been documented elsewhere,[1] we shall show here some new results for a three-dimensional lifting body.

Figures 1-3 display flowfield and heat transfer predictions for the FDL-5A lifting body that has been tested experimentally in a wind tunnel.[19] The computation is for a 5-deg angle of attack at Mach 10.2, a Reynolds number based on nose radius of 1.61×10^4, and a wall-to-stream temperature ratio of 0.63. Adequate accuracy was obtained by employing a perfect gas equation of state and a Sutherland viscosity law for air under the wind-tunnel test conditions. A zonal solution was obtained first for the nose region, followed by a time-iterative marching solution over the remainder of the body. The grid contained 20×40 (radial $\times$ circumferential) points in each cross-sectional marching plane. Figure 1 displays the body shape, grid, and computed shock-layer shape. As shown in Fig. 2, the predicted heat-transfer distributions along the windward and leeward centerlines are in good agreement with the experimental data, as is the circumferential heat transfer distribution at $x/L = 0.75$ displayed in Fig. 3. Aided by the solution-adaptive grid, reasonably accurate heat transfer predictions were obtained with the relatively sparse grid of 20 points in the body-normal direction.

Acknowledgments

This work was sponsored primarily by the Air Force Wright Aeronautical Laboratories under Contract F33615-83-C-3010. Portions also were performed under the Lockheed Independent Research and Development Program.

References

[1]Conti, R. J., "Test Cases for the HEARTS Computer Code," Air Force Wright Aeronautical Laboratories, Aerothermodynamics Branch, Wright-Patterson AFB, OH, informal technical information, various dates.

[2]Dorrance, W. H., *Viscous Hypersonic Flow,* McGraw-Hill, New York, 1962.

[3]Kays, W. M., *Convective Heat and Mass Transfer,* McGraw-Hill, New York, 1966.

[4]Bartlett, E. P., and Kendall, R. M., "An Analysis of the Coupled Chemically Reacting and Charring Ablator—Part III, Nonsimilar Solution of the Multicomponent Laminar Boundary Layer by an Integral Matrix Method," NASA CR-1062, June 1968.

[5]Thomas, P. D. and Lombard, C. K., "The Geometric Conservation Law and its Application to Fluid Dynamic Computations on Moving Grids," *AIAA Journal,* Vol. 17, No. 10, 1979.

[6]Chrusciel, G. T., "Evaluation of Slip Models for Rarefied Transitional Flow," Missile Systems Division, Lockheed Missiles & Space Co., Inc., Sunnyvale, CA, TM81-11/368, 1987.

[7]Baldwin, B. S., and Lomax, H., "Thin Layer Approximation and Algebraic Model for Separated Turbulent Flows," AIAA Paper 78-257, Jan. 1978.

[8]Thomas, P. D., and Neier, K.L., "Navier-Stokes Simulation of 3D Hypersonic Equilibrium Flows With Ablation," Vol. 1, Air Force Wright Aeronautical Lab., Wright-Patterson AFB, OH, AFWAL-TR-88-3020, 1988.

[9]Beam, R., and Warming, R. F., "An Implicit Factored Scheme for the Compressible Navier-Stokes Equation," *AIAA Journal,* Vol. 16, No. 4, 1978, pp. 393-402.

[10]Briley, W. R., and MacDonald, H., "Solution of the Multidimensional Compressible Navier-Stokes Equations by a Generalized Implicit Method," *Journal of Computational Physics,* Vol. 24, 1977.

[11]Pulliam, T. H., and Steger, J. L., "Implicit Finite-Difference Simulations of Three-Dimensional Compressible Flow," *AIAA Journal,* Vol. 18, No. 2, 1980, pp. 159-167.

[12]Thomas, P. D., "Numerical Method for Predicting Flow Characteristics and Performance of Nonaxisymmetric Nozzles—Theory," NASA CR-3147, Sept. 1979.

[13]Jameson, A., Schmidt, W., and Turkel, E., "Numerical Solutions of the Euler Equations by Finite Volume Methods Using Runge-Kutta Time-Stepping Schemes," AIAA Paper 81-1259, June 1981.

[14]Thomas, P. D., "Boundary Conditions for Implicit Solutions to the Compressible Navier-Stokes Equations on Finite Computation Domains," AIAA Paper 79-1447, July 1979.

[15]Svehla, R. A., and McBride, B. J., "FORTRAN IV Computer Program for Calculation of Thermodynamic and Transport Properties of Complex Chemical Systems," NASA TN D-7056, Jan. 1973.

[16]Schiff, L. B., and Steger, J. L., "Numerical Simulation of Steady Supersonic Viscous Flow," AIAA Paper 79-0130, Jan. 1979.

[17]Thomas, P. D., "Solution-Adaptive Grid for Viscous Hypersonic Flow," AIAA 87-0644, Jan. 1987.

[18]Thompson, J. F., "A Composite Grid Generation Code for General 3D Regions—The EAGLE Code," *AIAA Journal*, Vol. 26, No. 3, 1988, p. 271.

[19]Guard, F. L., and Schultz, H. D., "Preliminary Design and Experimental Investigation of the FDL-5A Unmanned High L/D Spacecraft, Part IV, Aerothermodynamics," Air Force Flight Dynamics Lab., Wright-Patterson AFB, OH, AFFDL-TR-68-24, Part IV, March 1968.

Clark H. Lewis
Associate Editor